

Effect of Gauge Length, Cross Sectional Area and Strain Measurement Methods on Stiffness Characterization of Fique Natural Fiber

Beatriz Casares Fernández^a and Meisam Jalalvand^b

^aMechanical and Aerospace Engineering, University of Strathclyde, Glasgow, UK; ^bEngineering and Physical Sciences, University of Southampton, Southampton, UK

ABSTRACT

Among different mechanical properties, stiffness of natural fibers is one of the most important and challenging properties to measure due to their irregular cross section area. In this paper, a direct strain measurement method is presented and applied to Fique (*Furcraea andina*) fibers. The results are compared against the conventional indirect strain measurement method commonly used in fiber characterization. The latter requires considering the system compliance, being particularly challenging for natural fibers with a wide variability among them. One solution to address this issue can be using gauge lengths of around 100 to 200 mm, which are longer than the ones typically used for the characterization of single fibers. Each fiber's cross section has been measured precisely, and the assumption that fibers have a circular cross section is studied. The Young's modulus of the tested Fique fibers is measured to be 17 GPa using indirect strain measurement, and it is found to increase with gauge length using direct strain measurement to 18 GPa for 100 mm length, for either area calculation approach. Fibers' area values show differences from assuming circularity to measure the cross-sectional area, but its impact on the Young's modulus is not significant when enough number of fibers is tested.

摘要

在不同的力学性能中，天然纤维的刚度是最重要和最具挑战性的性能之一，因为它们的横截面积不规则。本文提出了一种直接应变测量方法，并将其应用于Fique (*Furcraea andina*) 纤维。将结果与光纤表征中常用的传统间接应变测量方法进行了比较。后者需要考虑系统合规性，对于天然纤维来说尤其具有挑战性，因为它们之间存在很大的差异。解决这一问题的一种解决方案是使用约100至200毫米的标距长度，这比通常用于单纤维表征的标距长。精确测量了每根光纤的横截面，并研究了光纤具有圆形横截面的假设。使用间接应变测量法测得被测Fique纤维的杨氏模量为17GPa，使用直接应变测量法发现，对于任何一种面积计算方法，杨氏模量都随着标距长度的增加而增加，对于100 mm的长度，杨氏模量为18GPa。纤维的面积值显示了与假设圆形度来测量横截面积的差异，但当测试了足够数量的纤维时，其对杨氏模量的影响并不显著。


KEYWORDS

Fique; natural fibers; Young's modulus; indirect strain; direct strain; cross-sectional area

关键词

五;天然纤维;杨氏模量;间接应变;直接应变;横截面积

CONTACT Beatriz Casares Fernández  beatriz.casares-fernandez@strath.ac.uk  Mechanical and Aerospace Engineering, University of Strathclyde, 75 Montrose St, Glasgow G1 1XJ, Glasgow, UK

 Supplemental data for this article can be accessed online at <https://doi.org/10.1080/15440478.2024.2433056>

© 2024 The Author(s). Published with license by Taylor & Francis Group, LLC.

This is an Open Access article distributed under the terms of the Creative Commons Attribution-NonCommercial License (<http://creativecommons.org/licenses/by-nc/4.0/>), which permits unrestricted non-commercial use, distribution, and reproduction in any medium, provided the original work is properly cited. The terms on which this article has been published allow the posting of the Accepted Manuscript in a repository by the author(s) or with their consent.

Introduction

Natural fibers, used these days to make more sustainable composites, were from the beginning an important constituent of primitive and pre-historic composites, from mud-straw bricks to wood. While the search for stronger, lighter, and more durable materials (Bramwell 1976; Chawla 2012) has driven the evolution to the reinforced polymers, this development saw the other side of the coin, with researchers asking the same questions we are facing today (Hicks 1980): What can be done with composites when their life cycle finishes? Can they be recycled? (Henshaw, Owens, and Owens 1996; Hicks 1980). A lot of research has been going into the recycling route (Kennerley et al. 1998; Pakdel et al. 2021; Pickering 2006; Thomason, Yang, and Meier 2014) since landfilling and incineration (Krauklis et al. 2021) are not the first options given the volume of reinforced polymers coming from automotive, wind energy, and construction industries among other industries. Legislation started in the 90's by the European Economic Community legislating at the end of 1993 on the recycling of 50% by weight of the plastics used in automobiles and has been putting pressure on waste management of these type of materials with different Environmental Actions Plans that have been in place since then (Stewart 2009).

New sustainability trends across different industrial sectors are looking at natural fibers as one of the solutions to make composites more sustainable. Biodegradability, renewability, lightness, low cost, and socioeconomic impact in different communities are the main benefits of natural fibers (Mohanty et al. 2005; Muthu 2019). In fact, natural fibers have already been part of the aviation and automotive industries in the past century. When aluminum shortage was expected during World War II, in 1941, Gordon Aerolite developed a unidirectional flax fiber with phenolic resin composite for the Spitfire fuselage (Middleton 1992). Henry Ford was a pioneer when in 1942 he used hemp fibers for the development of his composite prototype car. After him, several companies in the automotive sector used natural fibers in their car components. Between 1950 and 1990, the East German Trabant used cotton, while coconut and jute are some of the fibers Daimler-Benz and Mercedes-Benz have explored in their car interiors since 1991 (Mohanty et al. 2005).

Some studies have explored flax/polyester for substituting E-glass fiber in small wind turbines blades (Shah, Schubel, and Clifford 2013) as well as bamboo composites in curved surfaces for structural loads (Pozo et al. 2017). Polylactic acid (PLA) reinforced with kenaf was used for developing mobile phone parts (Inoue et al. 2007). A combination of flax and carbon fibers has been used in different bicycle models, like the Schwinn Vestige and the 765 Optimum (Rakesh and Chaitanya Krishna 2019).

Other structural applications such as retrofitting, building rehabilitation and floor, wall, and roof insulating panels within civil engineering are also looking to sandwich panels or fiber reinforce composites where glass fiber can be substituted by natural fibers as flax. Sustainability efforts driving this change are challenged by natural fibers' hydrophilic nature, which has to be considered to ensure durability and mechanical performance under working conditions, as studied by Mak and Fam (Mak and Fam 2019a, 2019b, 2020). On top of this, other fields like electronics can benefit from the use of natural fibers and biopolymeric materials like cellulose and lignin (Irimia-Vladu and Sariciftci 2024) that can be sourced from fibers like fique as studied by Souza et al. (2017) in the production of membranes made from cellulose nanofibers. Young's modulus is one of the most important mechanical properties necessary for material characterization. It directly affects composite materials' Young's modulus, which is one of the key parameters in the design and analysis of structures. So far, the methodology used to find the tensile properties of manmade fibers has been applied to natural fibers (Adusumalli et al. 2019), e.g. ASTM standards D-3822-20 and C1557-20.

The Young's modulus measurement consists of longitudinal loading of the fiber, recording the applied extension to the fiber ends as well as the force. Measuring the fiber end extension using the loading machine is not accurate. The loading machine and the other components of the sample have a finite compliance and they deform with the applied load. Therefore, obtaining the fiber actual deformation requires accounting for this compliance. In the standard test method for measuring the

Young's modulus of fibers (ASTM-C1557-20, 2021), the fiber has to be mounted onto a paper tab that is cut before loading is applied. The fiber with the tab and the loading system are considered as two springs in series. By applying Hooke's law as explained by Rudeiros-Fernández (2016), it has been assumed that the compliance of the loading system does not change, but the stiffness of the fibers changes for different fibers with different cross-sections or lengths. This allows us to find the compliance of the system and consequently find the fibers' Young's modulus. At least three fiber gauge lengths must be tested for single fibers, so a linear regression can be applied to obtain the two springs' constants. In Figure 1, modified from the standard (ASTM-C1557-20 2021), it is shown how the Young's modulus corresponds to the inverse value of the fitted line slope, and the system compliance corresponds to the value where the fitted line intersects the vertical axis.

Depuydt et al. (2017) compared the Young's modulus of bamboo and flax fibers using both indirect and direct strain measurements using steel fibers as a reference to compare the accuracy of the different techniques. To measure the strain directly on the fibers, optical flags with a speckle pattern were attached to the fiber and their displacement was tracked using digital image correlation (DIC). The fiber strain was extracted based on the relative pixels' displacement. The conclusion of this work was that the measured Young's modulus from the indirect strain measurement method was 25% less than those found using the direct strain measurement method, arguing the inaccuracy of the assumption of a constant system compliance. In a similar work, Huether et al. (2018) attached fluorescent epoxy beads to 80 mm long glass fibers and applied the load in steps, allowing for higher resolution images to be taken to measure the strain directly. The limited number of studies carried out with direct strain measurements on single fibers indicates the experimental challenges. For instance, it is objectively difficult to apply mechanical extensometers on single fibers and applying visually trackable flags on natural fibers is not trivial, although their higher dimensions can ease the attachment of flags compared to synthetic fibers.

In addition to the challenges of handling individual fibers and measuring their strain, the natural fibers have much broader scatter in their dimensions and properties than manmade fibers due to different factors like harvest time, field retting time, climate and location (Liu et al. 2015, Bourmaud et

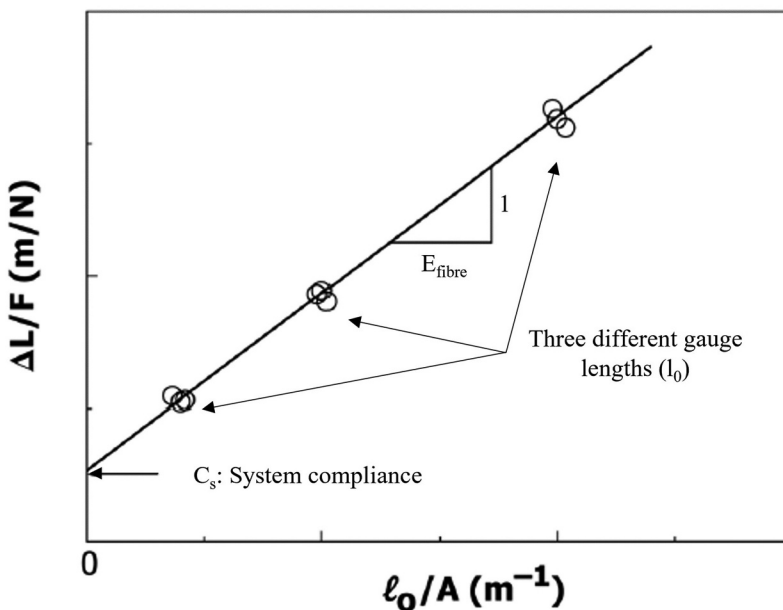


Figure 1. Calculation of the fiber's Young's modulus adapted from the standard (ASTM-C1557-20 2021) to highlight the requirement of at least three different gauge lengths.

al. 2016). However, this scatter is not only due to the intrinsic natural origin of these fibers but also due to the differences in the testing method and the factors affecting it, like the gauge length used; the use of single or technical fibers with potentially more damage during the processing; the loading rate; and the environment where the test is performed due to the hygroscopic nature of cellulose (Haag and Müssig 2016; Shah, Nag, and Clifford 2016).

Added to this, the intrinsic variability of natural fibers' cross section area and its measurement are a difficult challenge to overcome. In many studies (Stamboulis, Baillie, and Peijs 2001; De Rosa et al. 2010; Vincent, Cisse, and Lamine Boubakar 2012; Bastidas et al. 2022), the cross-section area is calculated by observing the fibers transversely under an optical microscope and assuming circularity of the cross-section. This is not necessarily correct in the case of natural fibers. Because of the impact the cross-section area value has on the calculation of tensile properties, different attempts have been made in order to improve the accuracy of cross-sectional area measurement in natural fibers by looking at the actual cross section, proving the oversimplification of the circularity assumption (Garat et al. 2018; Nitta et al. 2013; Thomason et al. 2011; Virk, Hall, and Summerscales 2010). To study the fibers' cross section circularity assumption and its effect on the measured Young's modulus on fique fiber, both techniques are used alongside direct and indirect strain measurement methods.

Few works have looked into fique tensile characterization (Delvasto et al. 2010; Gañán and Mondragon 2004; Gomez et al. 2020; Luna et al. 2017), but either single gauge length was used or details on how the test was performed are not clearly reported. On the work done by Muñoz-Blandón et al. (2022), fique fiber mechanical characterization is done to 50 mm-long textile fibers with 25 specimens. Bastidas et al. (2022) have also worked on characterizing fique fiber, but in this case through Dynamic Mechanical Analysis (DMA), at a length of 17.5 mm.

Modeling mechanical behavior of fique fiber reinforced composites requires more accurate characterization of fique fiber properties, beginning with the Young's modulus presented in this work. The work done by González-Estrada, Díaz, and Quiroga (2018) with woven material uses experimental data as input parameters to analyze the mechanical properties of the reinforced epoxy matrix. Also, as explained by Mulenga et al. (2021), different theories and modeling techniques have been developed to predict natural fiber composites behavior, helping to find appropriate applications for these materials, and more accurate fiber properties are necessary for such models.

This paper on stiffness characterization of fique fiber has three main pillars: first, measuring the cross sectional area of the fibers, both transversely and directly, and assessing the accuracy of the circularity assumption; second, using the direct and indirect strain measurement techniques to compare the values obtained for the Young's modulus to assess the validity of applying the compliance method when characterizing natural fibers; and third, considering five different gauge lengths, using significantly longer fiber lengths than the ones typically used for characterization.

Experiments

Materials and equipment

Fique fibers used in this study were provided by Compañía de Empaques, which uses them to produce coffee sacks and ropes among other products in Colombia. First, the fibers were brushed to remove organic residues and washed in lukewarm water. After that, fibers were wrapped around a square metallic plate and dried in an oven for three hours at 80°C, according to thermal analysis of fique, for which the range between 60 and 100°C corresponds to the release of moisture (Gañán and Mondragon 2004). This helps to straighten the fibers and makes sample preparation easier. Fibers were approximately cut to fit the 250 gr/m² card size for the five different gauge lengths of 10, 20, 40, 100 and 200 mm and mounted following (ASTM C1557-20 standard 2021).

Tensile tests were carried out using a Testometric M250–2.5CT testing machine with a 100 N load cell. The strain rate was established at 5% strain per minute and kept constant for all gauge lengths, so the applied displacement per min was proportional to the fiber gauge length.

For each fiber, Wintest analysis software that controls the Testometric testing machine recorded the load as a function of the crosshead displacement and time. Simultaneously, each test was recorded with a digital video camera Canon Legria HF G50 setup on a tripod at 50 cm from the sample, capturing 50 frames per second.

Sample preparation

Fibers were randomly selected and visually inspected to avoid fibers with obvious fraying or residue visible to the naked eye. Fibers were inserted in green beads of around 1 mm diameter and glued to them by using two components epoxy droplets deposited by a thin wire. The attachment of the fibers to the card was done using double-sided tape and later covered by epoxy resin to avoid slippage of the fiber during testing.

Area calculation

The fibers were transversely placed under a Leica microscope and the image was captured at x100 magnification to obtain the apparent diameter of the fibers.

For the shortest fiber lengths, 10, 20 and 40 mm, one picture of the midpoint was taken, while for the two longest gauge lengths of 100 and 200 mm, three pictures at the top, middle and bottom of the fibers were taken due to the significant length increase and the possibility of variation of cross section along the length. On each picture, three measurements of the apparent diameter were done using ImageJ software and then averaged. [Figure 2\(a\)](#) shows an example of three measurements taken from the transverse view. The area of the fiber was estimated using the average apparent diameter and assuming a circular cross section.

To find the true cross-sectional area (CSA) of the fibers, after the test, the two pieces of the broken fibers were cut out and glued to a card using Loctite Gel Superglue. The cards with the fibers were later placed in a circular mold, and transparent Epofix epoxy resin was poured into the mold to embed the fibers. After leaving the resin to cure for 24 hours at ambient temperature, the surface of the molds with the embedded fibers was ground at 300 rpm with progressively finer grit silicon carbide paper numbers 500, 800, 1200 and 2400. Polishing was done at 150 rpm, again with progressively finer diamond papers of 6, 3 and 1 micron(s) on a DP mol pad with the DP lubricant.

Fiber cross sections were photographed using an Olympus GX51 microscope at x200 magnification and later measured using ImageJ software. Two measurements were done per fiber as shown in [Figure 2\(b\)](#) using the fiber contour considering the whole section without distinguishing between fiber walls and lumen, as generally agreed ([Thomason et al. 2011](#)). An averaged value of the CSA was used for the modulus calculation.

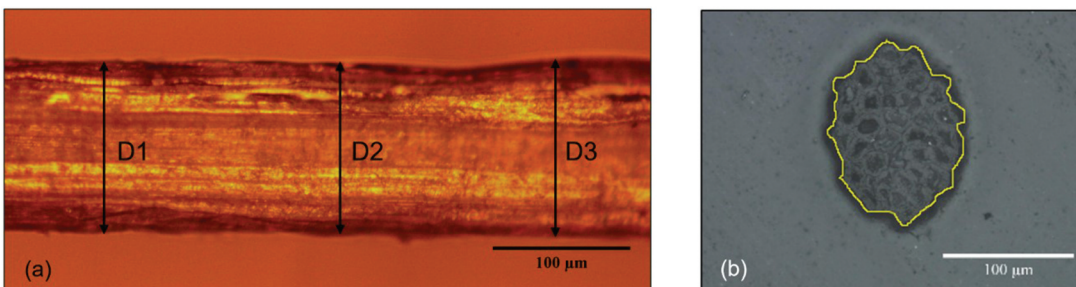


Figure 2. (a) Transversely observed apparent diameter at x100 magnification, with the three apparent diameter measurements for calculating the area assuming circularity. (b) Cross section area (CSA) measurement at x200 magnification with contour in yellow; both using ImageJ software.

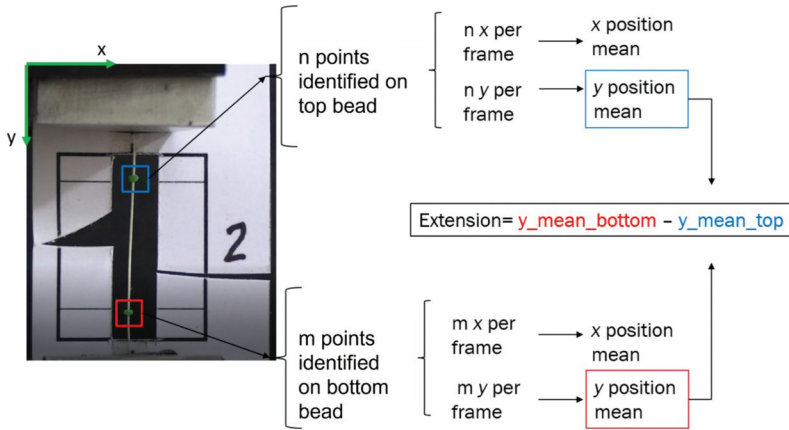


Figure 3. Flowchart of the MATLAB code for tracking the two beads attached to each tested fiber, where n and m are the number of points identified on each bead.

Direct strain measurement

The two beads on each fiber are assumed to move with the points on the fiber they are attached to, so by tracking their movement, the elongation of the fiber is captured. These beads, which are significantly shorter than the total length of the fibers, are assumed to be rigid solids.

The bead movement on every fiber was video recorded, and an in-house MATLAB code was developed to track the bead movement in a post processing stage of the captured videos. The video is opened in MATLAB, and the area occupied by each bead is manually selected. The *detectMinEigenFeatures* function recognizes n and m number of points on each bead using the *minimum eigenvalue* algorithm for all the video frames and calculates the average position for the top and bottom beads for every frame in pixels, as shown in Figure 3. The position of each bead for every frame is tracked by the Kanade–Lucas–Tomasi (KLT) algorithm (MathWorks 2019). The elongation is then calculated by finding the difference between the averaged movement of the beads in the y axis direction in pixels, allowing for the calculation of the average strain when divided by the initial distance between the beads in pixels. The data acquisition frequency of the tensile testing equipment is between 15 and 20 s^{-1} , while the video camera captures 50 frames per second. To match the data points between strain from the processed videos and force from the tensile machine, for every strain value, tensile force is found using a linear interpolation.

The stress values are found by dividing the force by the area. The slope of the initial linear part of the stress–strain curve for each fiber is used to find the Young–s modulus (Torayca 2003), with two values obtained for each fiber, one per area calculation method, as stress values change depending on the area used.

Results of fibers breaking very close to the beads or to the cardboard edges were discarded as well as those that showed slippage at the end tab during the test. This led to 24 fibers of 10 mm , 29 fibers of 20 mm , 50 fibers of 40 mm , 46 fibers of 100 mm and 49 fibers of 200 mm , considered as valid tests over a total of 306 fibers tested.

Results

First, the fiber area variation and the comparison between the two approaches for area calculation are presented. Secondly, the measurement of the elastic modulus by the indirect and direct strain measurement methods for different gauge lengths is presented.

Cross section area variation

Figure 4 shows the distributions of the area values obtained for the two approaches. When using the apparent diameter, a peak in the area values is seen for fibers with a cross sectional area between 10×10^3 and $15 \times 10^3 \mu\text{m}^2$; while for the CSA approach, the measured value has more uniform frequency 5×10^3 and $20 \times 10^3 \mu\text{m}^2$ with a relatively similar frequency. Assuming circularity does not accurately represent well the area of the fibers.

Table 1 shows the averaged area values (\bar{A}) for each method and the gauge length with their standard deviations and coefficients of variation. Circularity assumption from the apparent diameter is inaccurate, especially for short gauge lengths of 10, 20 and 40 mm when compared to the cross-sectional area. However, the difference between the transversely measured apparent diameter area and the direct cross-sectional area measurements reduces at longer gauge lengths. This is deemed to be since for longer fibers, 100 and 200 mm, measurements were taken at three different places along the fiber, leading to a more representative value of the fiber area when assuming circularity. Overall, the averaged area value from assuming circularity, $18.4 \times 10^3 \mu\text{m}^2$, is slightly higher than the one from the CSA measurement, $17.1 \times 10^3 \mu\text{m}^2$.

Figure 5 is a graphical comparison between the apparent diameter and cross-sectional area approaches, without distinguishing between gauge lengths, for a total of 198 fibers. The dashed line

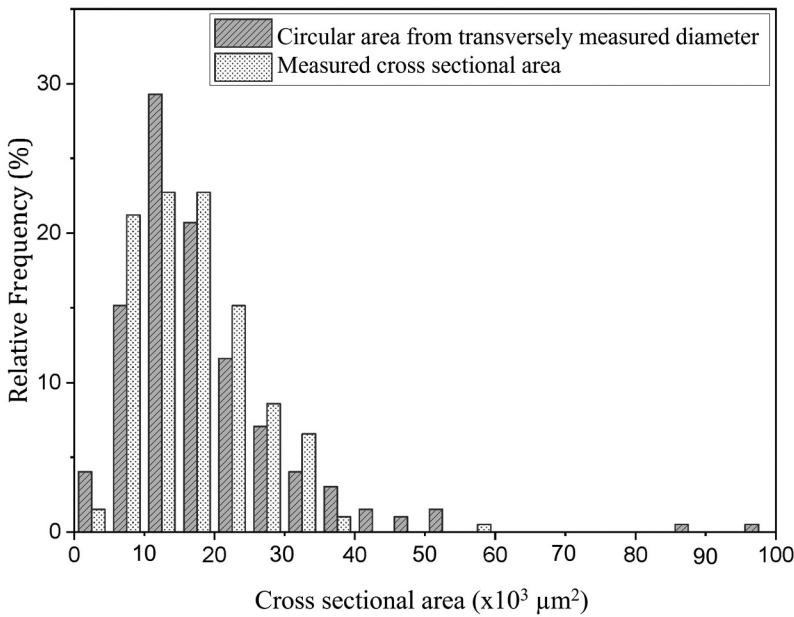


Figure 4. Fiber’s cross sectional area frequency intervals for the two area estimation approaches, assuming circularity from the apparent diameter and measuring the cross-sectional area at the failure point.

Table 1. Area obtained from the apparent diameter approach assuming circularity compared to the area measured by the cross-sectional area observation.

		10mmGL	20mmGL	40mmGL	100mmGL	200mmGL	Averaged
Average Area \bar{A} [$\times 10^3 \mu\text{m}^2$]	AD	30.6	23.9	14.9	17.1	13.6	18.4
	CSA	16.9	18.2	19.1	18.2	13.3	17.1
Standard deviation s [$\times 10^3 \mu\text{m}^2$]	AD	22.6	13.6	8.3	7.3	5.7	12.5
	CSA	6.6	6.3	8.7	9.7	6.1	8.1
Coefficient of variation (s/\bar{A}) [%]	AD	73.9	56.9	55.5	42.8	41.9	67.9
	CSA	39.1	34.7	45.7	53.6	45.8	47.4

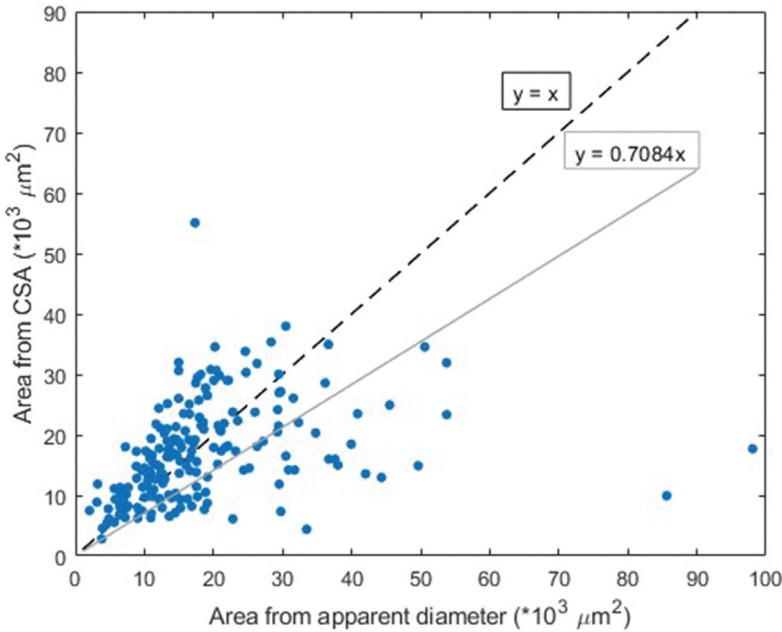


Figure 5. Fiber cross section area measured vs. area estimated by assuming circularity. The dashed line represents where the points would sit if both approaches gave the same values. The solid line represents the actual fitting, with a slight overestimation when the apparent diameter with circularity assumption is used over the cross-sectional area approach.

shows the location of points where both approaches would give the same area value. The solid line is the fitted line to the actual data. This shows that when not discerning by the gauge length, the apparent diameter approach for fiber cross sectional area measurement tends to overestimate the area value compared to the CSA observation as shown in the averaged value in [Table 1](#).

Young's modulus

Two methods of direct and indirect strain measurement for finding the Young's modulus of the fibers are discussed below.

Indirect strain measurement method

[Figure 6\(a\)](#) shows the results of the ASTM-C1557-20 standard method applied to all the valid tested fibers considering apparent diameter area measurement. [Figure 6\(b\)](#) shows the same standard applied using the CSA instead. The inverse of the slope of the line fitted to the data points represents the fibers average Young's modulus.

For both area measurement techniques, the fitted line has a similar slope, giving Young's modulus values of 17.3 GPa and 17.1 GPa, respectively.

The coefficient of determination, R^2 , for each line is shown in both graphs of [Figure 6](#). Higher values of R^2 are an indication of low variation in data, and this shows that the variation is higher when using the apparent diameter instead of CSA.

Direct strain measurement method

[Figure 7](#) shows how a line fitted to the initial part of the stress–strain curve and its slope, a , identified as the Young's modulus. The averaged value of Young's modulus, standard deviation, and coefficient of variation for every gauge length are given in [Table 2](#). Since fiber's area has a direct impact on the measured Young's modulus, two different values are provided: one using the measured apparent

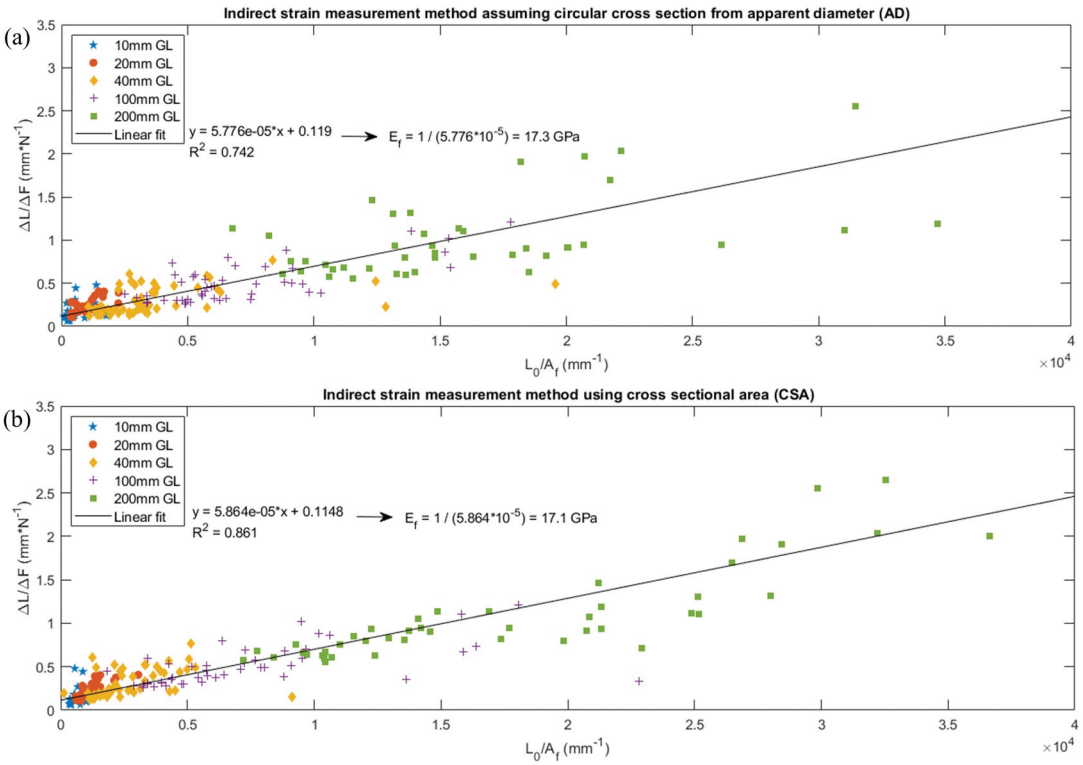


Figure 6. (a) Compliance theory applied by using area from the apparent diameter using circularity assumption of the fiber. Panel b shows the compliance theory applied by using the cross-sectional measured area of the fibers. The Young’s modulus of the fibers is the inverse value of the fitted slope, giving very close values for both cases, 17.3 and 17.1 GPa, respectively. The coefficient of determination R^2 is higher when using the cross-sectional area measured, suggesting a better fit for this case.

diameter for each fiber and another one using the measured CSA. **Figure 7** shows the stress–strain curve plotted with raw data as obtained from the equipment and as measured from the video. A toe shape can be seen at the beginning of it, which is associated with the fiber not being fully loaded. For visualization purposes and considering that the stress–strain curve theoretically starts in the origin, all curves have been shifted in the x-axis toward the origin, with the no loaded region removed.

As shown in **Table 2**, the values of the Young’s modulus increase with the increase in the gauge length for the apparent diameter approach. A similar trend is observed for the measured CSA approach, although this is not true for every single increase in gauge length.

Discussion

The obtained results show that the variability in fibers’ cross-sectional area is significant. Also, the significant difference between measured CSA and transversely measured apparent diameter along with the circularity assumption shows the inaccuracy of this approximation as was previously observed in other studies for different natural fibers (Virk, Hall, and Summerscales 2010; Thomason et al. 2011; Haag and Müssig 2016; Garat et al. 2018). For example, **Figure 4** shows a clear peak for the apparent diameter approach between 10 and $12 \times 10^3 \mu\text{m}^2$ of the area values. In contrast, the CSA approach gives similar area frequencies in a wider range between 5 and $20 \times 10^3 \mu\text{m}^2$.

Although the apparent diameter method is not an accurate method to give diameters of individual fibers, the average area values found using both methods are relatively close: 18.4 and $17.1 \times 10^3 \mu\text{m}^2$ for apparent diameter and CSA, respectively, as presented in **Table 1**. The difference between the two

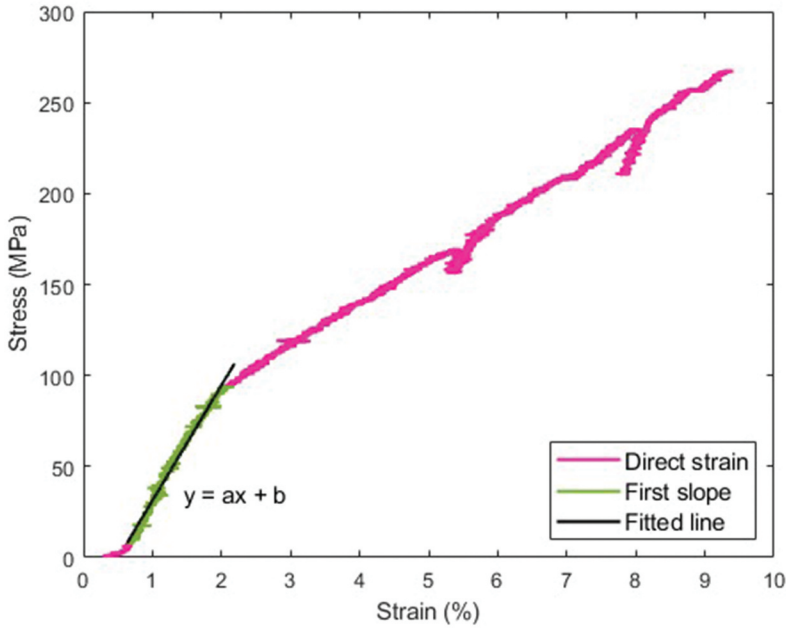


Figure 7. Stress–strain curve obtained from the direct strain measurement method, where the initial slope of the curve is used to calculate the Young’s modulus of the fiber by fitting a line of which slope is taken as the Young’s modulus, represented by a on the line equation.

Table 2. Young’s modulus values, standard deviation, and coefficient of variation for different gauge lengths from the direct strain measurement method.

		10mmGL	20mmGL	40mmGL	100mmGL	200mmGL
Average Young’s modulus \bar{E} [GPa]	AD	6.9	7.9	16.6	17.8	18.5
	CSA	9.5	8.3	13.1	18.7	18.4
Standard deviation s [GPa]	AD	5.7	5.2	8.3	6.2	6.3
	CSA	4.3	3.2	10.3	13.0	4.9
Coefficient of variation (s/\bar{E}) [%]	AD	82.1	66.1	49.9	34.7	33.9
	CSA	45.7	37.9	79.0	69.6	26.4

methods is more pronounced for the 10 and 20 mm gauge lengths with lower fiber numbers, suggesting that there is a minimum number for which assuming circularity tends to converge to the cross-sectional area measurement approach. In other words, if enough number of fibers is measured, it is deemed that overestimated area values are balanced by underestimated ones in the apparent diameter approach, leading to a relatively similar averaged value when compared with the CSA approach. The fact that there is still some tendency of overestimation in the former can be due to handling during the process of photographing the fibers transversely, with them tending to lay more on their wider axis.

Both area measurement approaches give similar values of Young’s modulus, around 17 GPa, when the indirect strain method is used. Our results showed that fibers longer than 40 mm are needed to achieve more reliable results and to correct the values obtained at lower gauge lengths especially when the circularity assumption is used. The Young’s modulus would be 39 GPa if only short fiber lengths of 10, 20 and 40 mm were used when assuming circularity, while it would stay around 19 GPa if the cross-section area measurement approach was to be used.

Longer fiber gauge lengths of 100 mm and 200 mm led to a higher number of valid tests. This is deemed to be the reason why both apparent diameter and direct cross sectional area measurements

resulted in similar Young’s modulus values. This leads to longer fibers having a more reliable outcome even when the apparent diameter approach is used, suggesting that this method can be used with longer gauge lengths by assuming circularity of the fibers with confidence.

The direct strain measurement presented gives higher values of Young’s modulus for gauge lengths 100 and 200 mm compared to shorter gauge lengths as presented in Table 2. The obtained stress–strain curves from the direct strain measurement were compared against the loading machine’s crosshead displacement as shown in Figure 8. Figure 9 shows the average maximum force tolerated by different fibers. The longer and the shorter fibers have similar maximum force. Figure 10 shows the

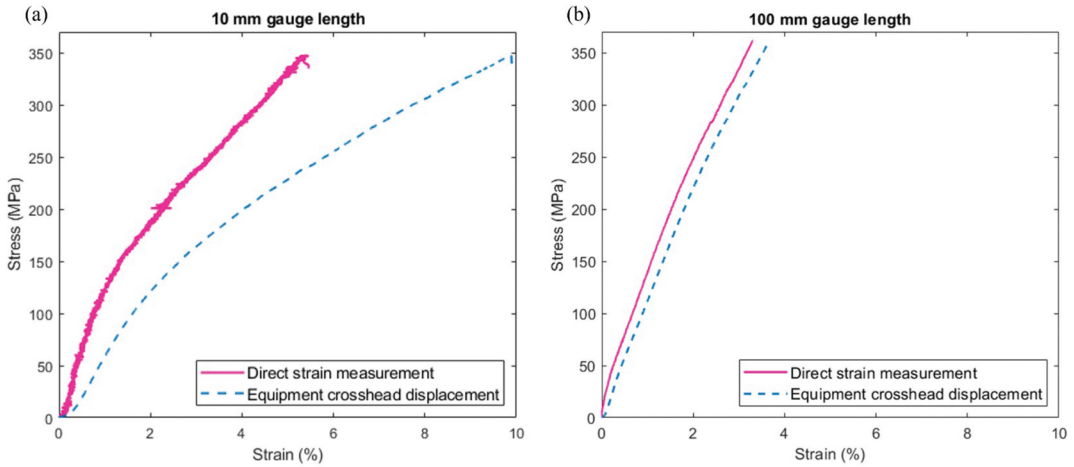


Figure 8. Two typical stress–strain curves of 10 and 100 mm fiber lengths for comparison. Both panels a and b show the differences between the direct strain measurement (solid line) vs. the equipment cross head displacement (dashed line), in both cases using the cross-sectional area (CSA).

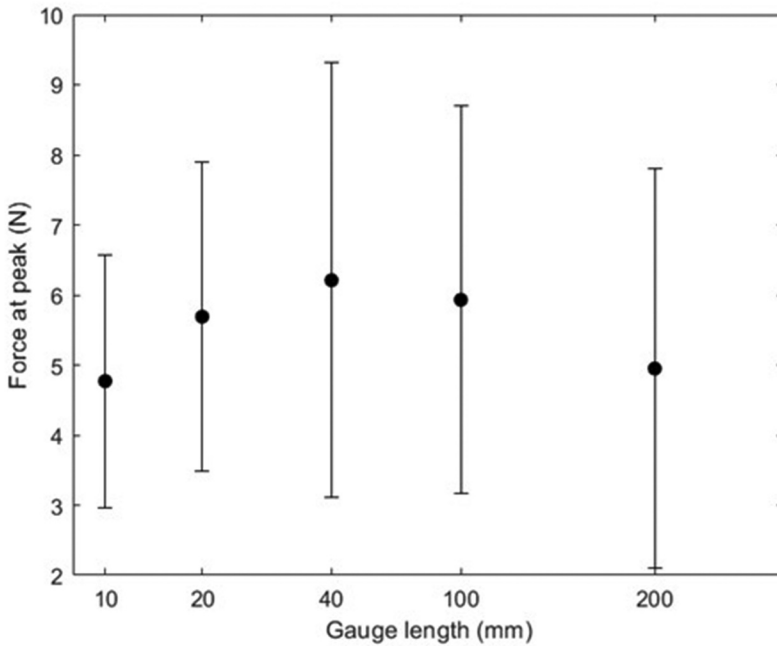


Figure 9. Average force values with the standard deviation for the different gauge lengths tested.

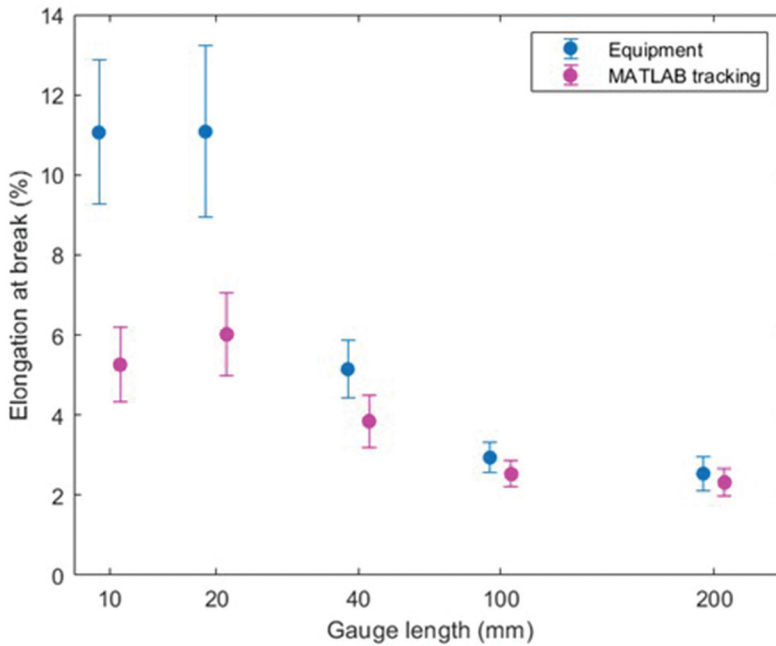


Figure 10. Average elongation at break for the different gauge lengths tested from both, direct strain measurement (MATLAB tracking) and the equipment crosshead displacement, showing how the difference between the two reduces with the gauge length increase, with overall values reducing with the gauge length increase.

average elongation at break for different gauge lengths and different strain measurement methods. The average maximum elongation found from the direct strain measurement and crosshead displacement are higher at shorter gauge length and reduces as the gauge length is increased. In other words, both methods show that longer fibers reach maximum forces similar to shorter ones at about half extension of the shorter fibers, as can be seen comparing CSA stress–strain curves using direct strain measurement of 10 mm and 100 mm gauge lengths in [Figure 8](#). The complexity of natural fibers makes their characterization challenging. Not only the area variation between the fibers but also the differences in the typical stress–strain curves for 10 and 100 mm shown in [Figure 8](#) suggest that non-linear behavior of the fibers is not neglectable. This nonlinearity is more significant when testing short fibers. The authors results show that at longer gauge lengths, different strain and cross-sectional area measurements give much closer results with less nonlinear stress–strain curves.

The Young’s modulus values obtained in this work, independently of the method, are, in general, higher than the ones found in the literature of 4, 8, 12, and 11.54 GPa ([Delvasto et al. 2010](#); [Gañán and Mondragon 2004](#); [Gomez et al. 2020](#); [Muñoz-Blandón et al. 2023](#)). These characterizations were made for 50 mm or unreported fiber length always assuming circularity of the fiber cross-sectional area with batches of 30 to 40 fibers. [Delvasto et al. \(2010\)](#) justifies this variation in the measured mechanical properties, as well as in the dimension changes along the fiber for its structural purpose depending on its position on the leaf and on the varying weight support requirements, which could partially explain the variation in the obtained Young’s modulus values. Variation in mechanical properties is known to happen under different growing conditions ([Liu et al. 2015](#)), but also the combined effect of shorter gauge lengths used in those studies and the circularity assumption can explain this difference in elastic modulus values. In the mechanical characterization done through DMA by [Bastidas et al. \(2022\)](#), the obtained Young’s modulus is higher than that reported in this work, with a value of 24.31 GPa.

The direct strain measurement method presented here can be applied to other natural fibers, like flax or jute, to understand their mechanical behavior and calculate more accurately their Young’s

modulus, or at least help to close the gap of values within the literature (Adusumalli et al. 2018; Hu et al. 2010; Depuydt et al., 2019). If the assumption of circularity is valid for different natural fibers and how it can be better measured needs to be studied for each of them, as done here (Soatthiyanon, Crosky, and Heitzmann 2022).

Conclusions

The achieved results in this work suggest:

- Direct strain measurement can be more easily done for natural fibers than for finer synthetic fibers due to their relatively large diameters. This can help remove the compliance of the testing equipment.
- Circularity assumption can potentially be used for the fique fibers if enough number of fibers are tested with fibers longer than those traditionally used, or at least with more than one gauge length. For transversely measured apparent diameter, having three measurements along the fiber length, as done for longer fibers, 100 and 200 mm, can help in reducing the scatter in the estimated cross-sectional area. This can ease the characterization process since measuring the apparent diameter is significantly easier and faster than measuring the CSA.
- The CSA measurement approach does not have a great impact on the Young's modulus measurement, when compared to the apparent diameter approach if enough number of fibers is tested.
- If only short fiber lengths are considered, CSA measurement is more accurate, reducing the error induced by the assumption of circularity, especially when the indirect strain measurement method is applied.
- The indirect strain measurement method gives a value of 17 GPa for the Young's modulus of fique fiber, independently from the applied area measurement approach.
- The direct strain measurement method shows an increasing trend in the Young's modulus values with the gauge length increase, which goes from 6.9 to 18.5 GPa for the apparent diameter approach and from 9.5 to 18.4 GPa for the CSA approach. Our interpretation is that fiber length needs to be significant enough, so the nonlinear stress–strain behavior of the fiber is not the dominant phenomenon.
- Having three pictures for the longer gauge lengths of 100 and 200 mm has helped in reducing the difference between the apparent diameter and the CSA approach. In the future, it is recommended to take three pictures even if short lengths are used in natural fiber characterization processes and the assumption of circularity is used, as it can help in obtaining a more representative area value.

Highlights

- Direct strain measurement has been done to fique fibers and compared to indirect strain measurement.
- The area of the cross section of fique has been measured by assuming circularity of it via a transversely measured and averaged diameter as well as by directly measuring the cross-sectional area after the tensile test, and both approaches are compared to assess the accuracy of the circularity assumption.
- The impact of the area measurement approach has been analyzed when evaluating the Young's modulus of fique as part of the mechanical characterization.
- Five different gauge lengths have been tested to understand the impact of fiber length on the tensile characterization of fique.

Acknowledgments

The authors acknowledge the financial supports provided by the Royal Academy of Engineering and the Newton Fund: Industry - Academia Partnership Programme, IAPP1/100149 in collaboration with the National University of Colombia. The fibers were provided by Compañía de Empaques through the National University of Colombia. The authors acknowledge the kind supports provided by Dr Juan Meza at the National University of Colombia, without which the completion of this work would have been impossible.

Disclosure statement

No potential conflict of interest was reported by the author(s).

Funding

The work was supported by the Royal Academy of Engineering [IAPP1/100149]; University of Strathclyde [Student Excellence Award (SEA) Studentship].

Notes on contributors

Beatriz Casares Fernández is currently a KTP Associate in Product Lifecycle Optimization and Carbon Footprint reduction within the University of Strathclyde (UoS). Part of the Advanced Composites Group within the same University for her PhD studies in natural fibers for composite materials. She graduated with a MSc in Advanced Mechanical Engineering with Energy Systems also at UoS after studying Aerospace Engineering at Technical University of Madrid (UPM).

Dr. Meisam Jalalvand is a Lecturer in Composite Materials and Structures within Engineering and Physical Sciences at the University of Southampton. His research interests include high performance hybrid composites as well as natural fiber and biodegradable composites with the aim of achieving better understanding, performance, safety and sustainability. These will help tackle urgent challenges, including global warming and plastic pollution.

References

- Adusumalli, R. B., K. Chethan Venkateshan, C. Kunchi, and S. R. Vadlamani. 2019. "Tensile Testing of Single Fibres." *Procedia Structural Integrity* 14:150–157. <https://doi.org/10.1016/j.prostr.2019.05.020>.
- Alain, M. Gibaud, and C. Baley. 2016. "Impact of the Seeding Rate on Flax Stem Stability and the Mechanical Properties of Elementary Fibres." *Industrial Crops and Products* 80: 17–25. <https://doi.org/10.1016/j.indcrop.2015.10.053>.
- ASTM-C1557-20. 2021. "Standard Test Method for Tensile Strength and Young's Modulus of Fibers." *ASTM International* 2008:1–11. <https://doi.org/10.1520/C1557-20.2>.
- Bastidas, K. G., M. F. R. Pereira, C. A. Sierra, and H. R. Zea. 2022. "Study and Characterization of the Lignocellulosic Fique (*Furcraea Andina* Spp.) Fiber." *Cellulose* 29 (4): 2187–2198. <https://doi.org/10.1007/s10570-021-04377-6>.
- Bourmaud, A., M. Gibaud, and C. Baley 2016. "Impact of the Seeding Rate on Flax Stem Stability and the Mechanical Properties of Elementary Fibres." *Industrial Crops and Products* 80: 17–25 <https://doi.org/10.1016/j.indcrop.2015.10.053>.
- Bramwell, M. 1976. *The International Book of Wood*, edited by M. Bramwell. London: Mitchell Beazley Publishers Limited, 156–168.
- Chawla, K. K. 2012. *Composite Materials: Science and Engineering. Composite Materials: Science and Engineering, Third Edition*. <https://doi.org/10.1007/978-0-387-74365-3>.
- Delvasto, S., E. F. Toro, F. Perdomo, and R. Mejía de Gutiérrez. 2010. "An Appropriate Vacuum Technology for Manufacture of Corrugated Fique Fiber Reinforced Cementitious Sheets." *Construction and Building Materials* 24 (2): 187–192. <https://doi.org/10.1016/j.conbuildmat.2009.01.010>.
- Depuydt, D., K. Hendrickx, W. Biesmans, J. Ivens, and A. W. van Vuure 2017. "Digital image correlation as a strain measurement technique for fibre tensile tests." *Composites. Part A, Applied Science and Manufacturing* 99: 76–83 <https://doi.org/10.1016/j.compositesa.2017.03.035>.
- Gañán, P., and I. Mondragon. 2004. "Fique Fiber-Reinforced Polyester Composites: Effects of Fiber Surface Treatments on Mechanical Behavior." *Journal of Materials Science* 39 (9): 3121–3128. <https://doi.org/10.1023/B:JMSc.0000025841.67124.c3>.

- Garat, W., S. Corn, N. Le Moigne, J. Beaugrand, and A. Bergeret. 2018. Analysis of the Morphometric Variations in Natural Fibres by Automated Laser Scanning: Towards an Efficient and Reliable Assessment of the Cross-Sectional Area." *Composites Part A, Applied Science and Manufacturing* 108:114–123. November. <https://doi.org/10.1016/j.compositesa.2018.02.018>.
- Gomez, T. S., S. Zuluaga, M. Jimenez, M. D. L. Á. Navacerrada, M. D. M. Barbero-Barrera, D. de la Prida, A. Restrepo-Osorio, and P. Fernández-Morales. 2020. "Evaluation of Colombian Crops Fibrous Byproducts for Potential Applications in Sustainable Building Acoustics." *Polymers* 13 (1): 101. <https://doi.org/10.3390/polym13010101>.
- González-Estrada, O. A., G. Díaz, and J. Quiroga. 2018. "Mechanical Response and Damage of Woven Composite Materials Reinforced with Fique." *Key Engineering Materials* 774 KEM, 143–148. <https://doi.org/10.4028/www.scientific.net/KEM.774.143>.
- Haag, K., and J. Müssig. 2016. "Scatter in Tensile Properties of Flax Fibre Bundles: Influence of Determination and Calculation of the Cross-Sectional Area." *Journal of Materials Science* 51 (17): 7907–7917. <https://doi.org/10.1007/s10853-016-0052-z>.
- Henshaw, J. M., A. D. Owens, and A. D. Owens. 1996. "An Overview of Recycling Issues for Composites Materials." *Journal of Thermoplastic Composite Materials* 9 (1): 4–20. <https://doi.org/10.1177/089270579600900102>.
- Hicks, J. P. 1980. "A Stronger Future for Composites." *Business Technology, The New York Times*, August 8, 1980. <https://www.nytimes.com/1990/08/08/business/business-technology-a-stronger-future-for-composites.html>.
- Hu, W., M. T. Ton-That, F. Perrin-Sarazin, and J. Denault. 2010. "An Improved Method for Single Fiber Tensile Test of Natural Fibers." *Polymer Engineering & Science* 50 (4): 819–825. <https://doi.org/10.1002/pen.21593>.
- Huether, J., P. Rupp, I. Kohlschreiber, and K. A. Weidenmann. 2018. "An Enhanced Method to Determine the Young's Modulus of Technical Single Fibres by Means of High Resolution Digital Image Correlation." *Measurement Science and Technology* 29 (4). <https://doi.org/10.1088/1361-6501/aaa0bb>
- Inoue, K., S. Serizawa, M. Yamashiro, and M. Iji. 2007. "Highly Functional Bioplastics (PLA Compounds) Used for Electronic Products." *6th International IEEE Conference on Polymers and Adhesives in Microelectronics and Photonics, Polytronic 2007, Proceedings*: 73–76. <https://doi.org/10.1109/POLYTR.2007.4339141>.
- Irimia-Vladu, M., and N. S. Sariciftci. 2024. "Natural Polymers for Emerging Technological Applications: Cellulose, Lignin, Shellac and Silk." In *Polymer International*, John Wiley and Sons Ltd. <https://doi.org/10.1002/pi.6697>.
- Kennerley, J. R., R. M. Kelly, N. J. Fenwick, S. J. Pickering, and C. D. Rudd. 1998. "The Characterisation and Reuse of Glass Fibres Recycled from Scrap Composites by the Action of a Fluidised Bed Process." *Composites Part A, Applied Science and Manufacturing* 29 (7): 839–845. [https://doi.org/10.1016/S1359-835X\(98\)00008-6](https://doi.org/10.1016/S1359-835X(98)00008-6).
- Krauklis, A. E., C. W. Karl, A. I. Gagani, and J. K. Jørgensen. 2021. "Composite Material Recycling Technology—State-of-the-art and Sustainable Development for the 2020s." *Journal of Composites Science* 5 (1): 28. <https://doi.org/10.3390/jcs5010028>.
- Liu, M., D. Fernando, G. Daniel, B. Madsen, A. S. Meyer, M. Tutor Ale, and A. Thygesen. 2015. "Effect of Harvest Time and Field Retting Duration on the Chemical Composition, Morphology and Mechanical Properties of Hemp Fibers." *Industrial Crops and Products* 69:29–39. <https://doi.org/10.1016/j.indcrop.2015.02.010>.
- Luna, P., A. Mariño, J. Lizarazo-Marriaga, and O. Beltrán. 2017. "Dry Etching Plasma Applied to Fique Fibers: Influence on Their Mechanical Properties and Surface Appearance." *Procedia Engineering* 200:141–147. <https://doi.org/10.1016/j.proeng.2017.07.021>.
- Mak, K., and A. Fam. 2019a. "Freeze-Thaw Cycling Effect on Tensile Properties of Unidirectional Flax Fiber Reinforced Polymers." *Composites Part B Engineering* 174:106960. October. <https://doi.org/10.1016/j.compositesb.2019.106960>.
- Mak, K., and A. Fam. 2019b. "Performance of Flax-FRP Sandwich Panels Exposed to Different Ambient Temperatures." *Construction and Building Materials* 219 (September): 121–130. <https://doi.org/10.1016/j.conbuildmat.2019.05.118>.
- Mak, K., and A. Fam. 2020. "The Effect of Wet-Dry Cycles on Tensile Properties of Unidirectional Flax Fiber Reinforced Polymers." *Composites Part B Engineering* 183:107645. February. <https://doi.org/10.1016/j.compositesb.2019.107645>.
- MathWorks. 2019. "Computer Vision Toolbox." *Release 2019a*. <https://www.mathworks.com/products/computer-vision.html>.
- Middleton, D. H. 1992. "Composite Developments in Aircraft Structures—Part 1." *Aircraft Engineering and Aerospace Technology* 64 (5): 2–8. <https://doi.org/10.1108/eb037234>.
- Mohanty, Amar, M. Misra, L. Drzal, S. Selke, B. Harte, and G. Hinrichsen. 2005. "Natural Fibers, Biopolymers, and Biocomposites." In *Natural Fibers, Biopolymers, and Biocomposites*, CRC Press. <https://doi.org/10.1201/9780203508206.ch1.Mulenga>.
- Mulenga, T. K., A. U. Ude, and C. Vivekanandhan. "(2021)." Techniques for Modelling and Optimizing the Mechanical Properties of Natural Fiber Composites: A Review. In *Fibers*. (Vol. 9 (Issue 1): pp. 1–17). MDPI AG. <https://doi.org/10.3390/fib9010006>.
- Muñoz-Blandón, O., M. Ramírez-Carmona, L. Rendón-Castrillón, and C. Ocampo-López. 2023. "Exploring the Potential of Fique Fiber as a Natural Composite Material: A Comprehensive Characterization Study." *Polymers* 15 (12): 2712. <https://doi.org/10.3390/polym15122712>.
- Muthu, S. S. 2019. *Green Composites Processing, Characterisation and Applications for Textiles*. https://books.google.com/books/about/Green_Composites.html?hl=es&id=yzBPzQEACAAJ%0Ahttp://www.springer.com/series/13111.

- Nitta, Y., K. Goda, J. Noda, and W. Il Lee. 2013. "Cross-Sectional Area Evaluation and Tensile Properties of Alkali-Treated Kenaf Fibres." *Composites Part A, Applied Science and Manufacturing* 49:132–138. <https://doi.org/10.1016/j.compositesa.2013.02.003>.
- Pakdel, E., S. Kashi, R. Varley, and X. Wang. 2020. Recent Progress in Recycling Carbon Fibre Reinforced Composites and Dry Carbon Fibre Wastes." *Resources, Conservation & Recycling* 166:105340. December. <https://doi.org/10.1016/j.resconrec.2020.105340>.
- Pickering, S. J. 2006. "Recycling Technologies for Thermoset Composite Materials-Current Status." *Composites Part A, Applied Science and Manufacturing* 37 (8): 1206–1215. <https://doi.org/10.1016/j.compositesa.2005.05.030>.
- Pozo Morales, A., A. Güemes, A. Fernandez-Lopez, V. C. Valero, and S. de La Rosa Llano 2017. "Bamboo-Polylactic Acid (PLA) Composite Material for Structural Applications." *Materials* 10 (11).
- Rakesh, P., and N. Chaitanya Krishna. 2019. "Potential and Applications of Green Composites in Industrial Space." *Materials Today: Proceedings* 22:2041–2048. <https://doi.org/10.1016/j.matpr.2020.03.218>.
- Rosa, J. M. Kenny, I. M. De, J. Maria Kenny, D. Puglia, C. Santulli, and F. Sarasini. 2010. "Morphological, Thermal and Mechanical Characterization of Okra (*Abelmoschus Esculentus*) Fibres as Potential Reinforcement in Polymer Composites." *Composites Science and Technology* 70 (1): 116–122. <https://doi.org/10.1016/j.compscitech.2009.09.013>.
- Rudeiros-Fernández, J. L. 2016. *Investigation of the Mechanical Performance of Natural Fibres and Their Composites.* PhD thesis, University of Strathclyde.
- Shah, D. U., R. K. Nag, and M. J. Clifford. 2016. "Why Do We Observe Significant Differences Between Measured and 'Back-Calculated' Properties of Natural Fibres?" *Cellulose* 23 (3): 1481–1490. <https://doi.org/10.1007/s10570-016-0926-x>.
- Shah, D. U., P. J. Schubel, and M. J. Clifford. 2013. "Can Flax Replace E-Glass in Structural Composites? A Small Wind Turbine Blade Case Study." *Composites Part B Engineering* 52:172–181. <https://doi.org/10.1016/j.compositesb.2013.04.027>.
- Soatthiyanon, N., A. Crosky, and M. T. Heitzmann. 2022. "Comparison of Experimental and Calculated Tensile Properties of Flax Fibres." *Journal of Composites Science* 6 (4): 100. <https://doi.org/10.3390/jcs6040100>.
- Souza, S. F., A. L. Leao, C. B. Lombello, M. Sain, and M. Ferreira. 2017. "Cytotoxicity Studies of Membranes Made with Cellulose Nanofibers from Fique Macrobundles." *Journal of Materials Science* 52 (5): 2581–2590. <https://doi.org/10.1007/s10853-016-0551-y>.
- Stamboulis, A., C. A. Baillie, and T. Peijs. 2001. "Effects of Environmental Conditions on Mechanical and Physical Properties of Flax Fibers." *Composites - Part A: Applied Science and Manufacturing* 32 (8): 1105–1115. [https://doi.org/10.1016/S1359-835X\(01\)00032-X](https://doi.org/10.1016/S1359-835X(01)00032-X).
- Stewart, R. 2009. "Legislation for Recycling Waste Composites." *Management, Recycling and Reuse of Waste Composites*: 20–38. <https://doi.org/10.1533/9781845697662.1.20>.
- Thomason, J. L., J. Carruthers, J. Kelly, and G. Johnson. 2011. "Fibre Cross-Section Determination and Variability in Sisal and Flax and Its Effects on Fibre Performance Characterisation." *Composites Science and Technology* 71 (7): 1008–1015. <https://doi.org/10.1016/j.compscitech.2011.03.007>.
- Thomason, J. L., L. Yang, and R. Meier. 2014. "The Properties of Glass Fibres After Conditioning at Composite Recycling Temperatures." *Composites Part A, Applied Science and Manufacturing* 61:201–208. <https://doi.org/10.1016/j.compositesa.2014.03.001>.
- Torayca. 2003. "Ty-030B-01 Test Method Method for Determination of Tensile Strength Tensile Modulus of Elasticity, and Elongation at Break."
- Vincent, P., O. Cisse, and M. Lamine Boubakar. 2012. "Influence of Environmental Relative Humidity on the Tensile and Rotational Behaviour of Hemp Fibres." *Journal of Materials Science* 47 (7): 3435–3446. <https://doi.org/10.1007/s10853-011-6191-3>.
- Virk, A. S., W. Hall, and J. Summerscales. 2010. "Physical Characterization of Jute Technical Fibers: Fiber Dimensions." *Journal of Natural Fibers* 7 (3): 216–228. <https://doi.org/10.1080/15440478.2010.504389>.